J MATER RES TECHNOL. 2019;xxx(xx):xxx–xxx

Available online at www.sciencedirect.com

jmr&t Journal of Materials Research and Technology

www.jmrt.com.br

Original Article

Experimentation and analysis of powder injection molded Ti10Nb10Zr alloy: a promising candidate for electrochemical and biomedical application

Isıl Yemisci[a], *Ozal Mutlu*[b], *Nagihan Gulsoy*[b], *Kate Kunal*[c], *Sundar Atre*[c], *H. Ozkan Gulsoy*[c,d,*]

[a] *Marmara University, Inst. Graduate Studies Pure and Applied Sci., 34722, Istanbul, Turkey*
[b] *Marmara University, Faculty of Art and Sciences, Biology Dep., 34722 Istanbul, Turkey*
[c] *Materials Innovation Guild, University of Louisville, Louisville, KY 40292, USA*
[d] *Marmara University, Technology Faculty, Metall. And Mater. Eng., 34722, Istanbul, Turkey*

ARTICLE INFO

Article history:
Received 7 January 2019
Accepted 24 August 2019
Available online xxx

Keywords:
Powder injection molding
Titanium alloy
Sintering
Mechanical properties
Biocompatible

ABSTRACT

This paper describes the microstructural, mechanical and corrosion properties of injection molded Ti10Nb10Zr alloys. Ti10Nb10Zr powder was injection molded with wax-based binder. The critical powder loading for injection molding was 55 vol% for feedstock. Binder debinding was performed in solvent and thermal method. After debinding the samples were sintered at different temperatures and times in vacuum atmosphere (10^{-5} mbar) to obtain fully dense parts. Metallographic studies were conducted to determine the extent of densification and the corresponding microstructural changes. The electrochemical property and biocompatibility of the sintered samples were performed electrochemically, by self-body-fluid immersion tests and cell culture experiments. The results show that Ti10Nb10Zr alloys could be sintered to a maximum 99% of theoretical density. Maximum ultimate tensile strength, elongation and hardness obtained were 748 MPa, 14.3 and 114 HRB respectively at 1500 °C for 3 h. Additionally, the sintered Ti10Nb10Zr alloys exhibited high mechanical and corrosion properties in a physiological environment.

1. Introduction

Powder injection molding (PIM) is a novel manufacturing process, which combines plastic injection molding and conventional powder metallurgy (PM) technologies. The PIM process is composed of four sequential steps; mixing of the powder and organic binder, injection molding, debinding (binder removal), and sintering. PIM effectively combines the advantages of plastic injection molding with the versatility of traditional powder metallurgy to manufacture highly complex parts of small size, with tight tolerances, at low production cost and high volumes. The PIM process overcomes the

* *Corresponding author.*
E-mail: ogulsoy@marmara.edu.tr (H. Ozkan Gulsoy).
https://doi.org/10.1016/j.jmrt.2019.08.046

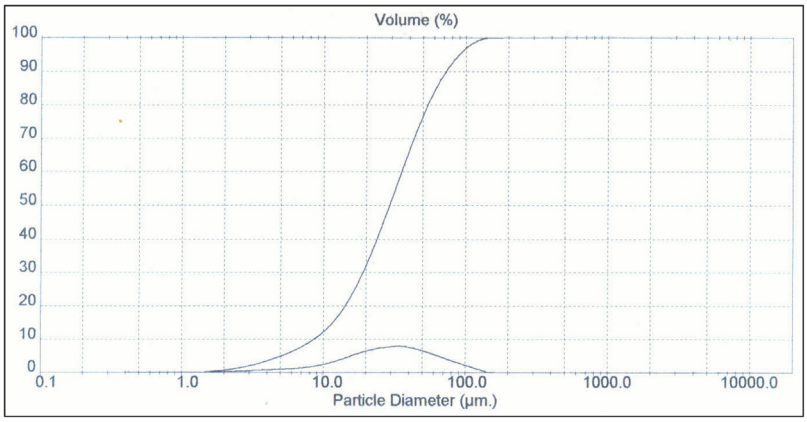

Fig. 1 – Cumulative particle size distributions for Ti powder.

shape limitation of traditional powder compaction, the cost of machining, the productivity limits of isostatic pressing and slip casting, and the defect and tolerance limitations of conventional casting. Mechanical properties of a well-processed powder injection molded material are indistinguishable from cast and wrought material [1–4].

Titanium and its alloys are generally preferred to stainless steels and Co–Cr alloys because of their low density, superior biocompatibility and corrosion resistance, good mechanical properties, and low elastic modulus [2,5]. Currently, titanium alloys are designed using non-toxic components such as Nb, Zr, Ta, Sn, In, and Mo, which tend to form a single BCC phase in the structure [6]. Compared with the classic early biomedical materials, including Ti-6Al-4V, CoCrMo and 316 l stainless steels, the new type of titanium alloys feature improved mechanical properties and corrosion resistance.

The first generation of α + β titanium alloys such as Ti6Al4V, Ti6Al7Nb and Ti5Al2.5Fe are already in use as bone implants in orthopedic applications but offer high modulus compared to bone [5–9]. In recent years, second generation near β and β type titanium alloys have been developed for bio-applications in order to avoid the "stress shielding" effect caused by the modulus mismatch between the implant and the bone [8,9]. As an example of second generation near β titanium alloy, TiNbZr was formulated in early 1990 to be used in bio-applications due to its low Young's modulus (40–80 GPa) and its non-toxic composition and superior corrosion resistance when compared to first generation titanium alloys such as Ti6Al4V and Ti6Al7Nb alloys [10].

Lately, low-modulus β titanium alloys containing chemical elements that are nontoxic and non-allergic to human body are currently being investigated as potential options for next generation of metallic implant materials [11,12]. Nb and Zr elements generally tend to be non-toxic and non-allergic to human body [14,15]. Furthermore, recent studies indicate that by adjusting the Nb and Zr alloying elements concentration in titanium alloys can create low elastic modulus β type Ti alloys with high strength that perform well in bio-applications [16,17]. One such titanium alloy is the Ti10Nb10Zr alloy where niobium is added as it acts as a beta-phase stabilizer. Whereas the other alloying element, zirconium is isomorphous with both the α and β phases of titanium. A combination of these two alloying elements has made it possible to develop a structure that is a "near" beta phase supposedly possessing a superior corrosion resistance over the α + β phase alloys, with enough alpha phase present in the final structure to provide the necessary mechanical strength.

In spite of Ti and its alloys having exceptional biocompatibility and mechanical properties their end products tend to be costly. A common reason for this is due to high starting powders costs and fabrication of 3-dimentional (3D) products that are complex in shape with traditional manufacturing process such as machining and casting increases the overall costs. Alternatively, PIM can be used to fabricate many Ti and Ti alloys 3D products in a cost effective way as it can achieve shape complexity, maximum material utilization, and near full final density compared to traditional manufacturing processes. Previous investigations on injection molded Ti and Ti alloys focused on the effect of powder characteristics (gas and water atomized mixed powder), sintering temperature, sintering time, heat treatment, residual carbon and oxygen content on microstructure. However, microstructural and mechanical properties of injection molded Ti10Nb10Zr powder have not been examined [15–25]. In addition, new types of titanium alloys with low elastic modulus have been tried in some studies [6]. All these studies have shown that new types of titanium alloys with low elastic modulus (80–94 GPa) and non-toxic can be developed.

The present work performs a comprehensive investigation to investigate the effect of sintering parameters on the sintering behavior, mechanical properties, electrochemical properties and biocompatibility properties of powder injection molded Ti10Nb10Zr alloys. Metallographic techniques were employed to sintered tensile bars to investigate the sintering behaviors. Additionally, tensile and hardness properties of the sintered products were evaluated at sintered conditions. Furthermore, the sintered samples were characterized for their corrosion resistance in two different environments: a salt solution (3.5% NaCl) and artificial saliva solution (ASS) using potentiodynamic polarization. Bioactivity of the all samples in a self-body-fluid (SBF) was investigated. Sintered samples were implanted in fibroblast culture for biocompatibility evaluations were carried out. Powder morphology, fracture surfaces of molding and sintered samples, surfaces after

Please cite this article in press as: Yemisci I, et al. Experimentation and analysis of powder injection molded Ti10Nb10Zr alloy: a promising candidate for electrochemical and biomedical application. J Mater Res Technol. 2019. https://doi.org/10.1016/j.jmrt.2019.08.046

immersion in SBF and proliferation of cells were analyzed under scanning electron microscope.

2. Experimental procedures

2.1. Test materials and fabrication method

In this study, HDH Ti sponge powder provided by Phelly Materials was used. The Nb and Zr powder was obtained from Alfa Aesar. Particle size distributions of Ti powder were determined on Malvern Mastersizer equipment and given in Fig. 1. Morphology of the Ti, Nb and Zr powders observed using SEM is given Fig. 2. All powders are irregular in shape. The powder characteristics and chemical properties of Ti, Nb, and Zr powders used in this study are given Table 1. To protect the powders from oxidation, all of the materials were stored in an argon atmosphere before mixing, and molding. Final compositions of samples were adjusted to give the Ti10Nb10Zr composition.

A multiple-component binder system consisting of paraffin wax, polypropylene, carnauba wax, and stearic acid was used. Feedstock was prepared at 175 °C with the binder melted first and then powder blend added incrementally. The powder loading in this mixture was 55 vol%. Rheological behavior of the Ti10Nb10Zr feedstocks was measured by using a rotational viscometer Physica MCR51 (Anton-Paar) at shear rates from10 to 1000 s^{-1} at 130–170 °C. The value of viscosity is given based on the shear stress divided by the shear rate. These feedstocks were injected using a 12.5 MPa specially made injection-molding machine to produce tensile (MPIF 50) test specimens. The melt temperature was 175 °C, the mold temperature was kept at 35–40 °C and cycle time was 20 s.

Debinding was conducted in a two-step solvent/thermal operation. Green parts were solvent debound at 60 °C for 8 h in heptane, followed by thermal debinding step by step at 2 °C/min to 600 °C for 1 h and pre-sintered at 5 °C/min to 900 °C for 1 h in a high purity argon atmosphere. The sintering cycle applied to the samples was as follows; samples were heated to 1100 °C at a rate of 10 °C/min, then the samples were heated to different sintering temperatures of 1100 °C, 1200 °C, 1300 °C, 1400 °C and 1500 °C at a rate of 5 °C/min and they were held at maximum temperature for 1, 2, 3 h in vacuum (10^{-5} mbar).

2.2. Physical and mechanical tests

The densities of the sintered samples were measured by means of the Archimedes water-immersion method. For metallographic examination, samples were cut from the center of the each sintered tensile test bar. A Kroll reagent (3 ml HF, 6 ml HNO_3 in 100 ml H_2O) was used to etch the samples for optical metallography. All tensile tests were performed using Zwick 2010 mechanical tester at a constant crosshead speed of 1 mm/min (25 mm gauge length). The hardness tests were performed using an Instron-Wolpert Dia Testor 7551 at HRB scale. At least three specimens were tested under the same conditions to guarantee the reliability of the results. The powder morphologies and fracture surfaces of molding and sintering samples were examined using a scanning electron microscope (FEI-Srion).

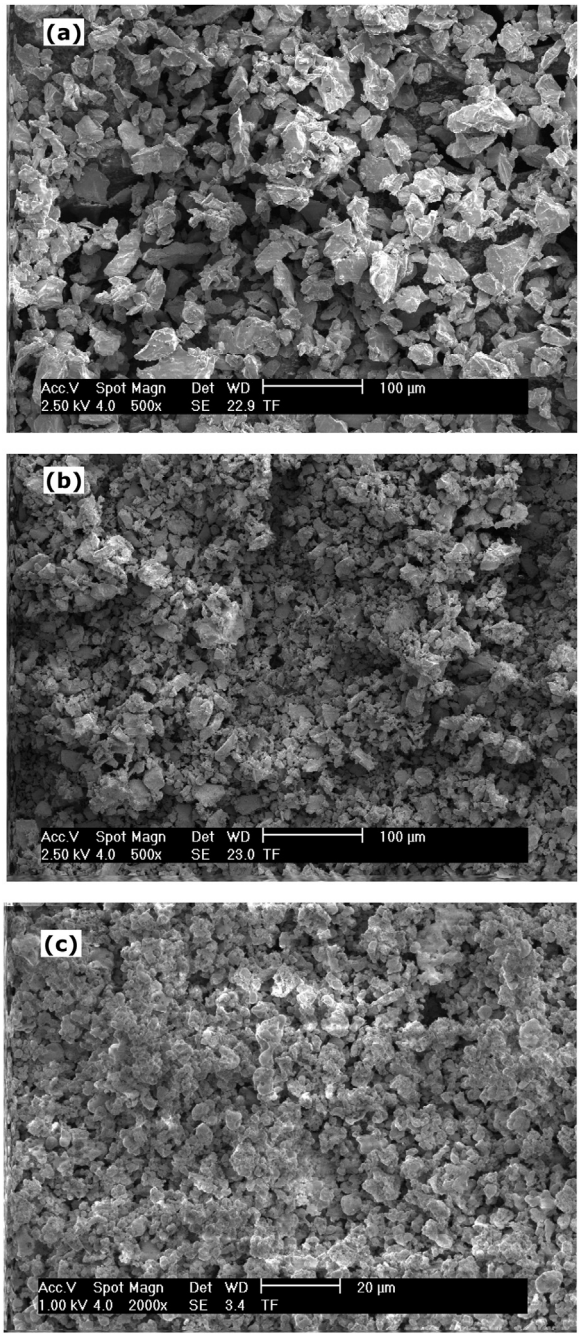

Fig. 2 – Particle morphologies of a) Ti, b) Nb and c) Zr powder.

Table 1 – Powder characteristic of Ti, Nb and Zr powders.

Item	Ti	Nb	Zr
Melting point, °C	1670	2468	1850
Vendor	Phelly Mater.	Alfa Aesar	Alfa Aesar
Shape	Irregular	Irregular	Irregular
Particle size			
D_{10}	16.05	3.52	1.95
D_{50}	32.69	8.53	6.97
D_{90}	57.15	21.28	26.72
Pycn. density, g/cm^3	4.51	8.42	6.53
Purity, %	Commercial purity	99.9	99.9

Please cite this article in press as: Yemisci I, et al. Experimentation and analysis of powder injection molded Ti10Nb10Zr alloy: a promising candidate for electrochemical and biomedical application. J Mater Res Technol. 2019. https://doi.org/10.1016/j.jmrt.2019.08.046

Table 2 – Ion concentrations of the SBF and human blood plasma (mmol/L).

	Na^+	K^+	Ca^{2+}	Mg^{2+}	HCO_3^-	Cl^-	HPO_4^{2-}	SO_4^{2-}
Blood plasma	142.0	5.0	2.5	1.5	27.0	103.0	1.0	0.5
SBF	142.0	5.0	2.5	1.5	4.2	147.8	1.0	0.5

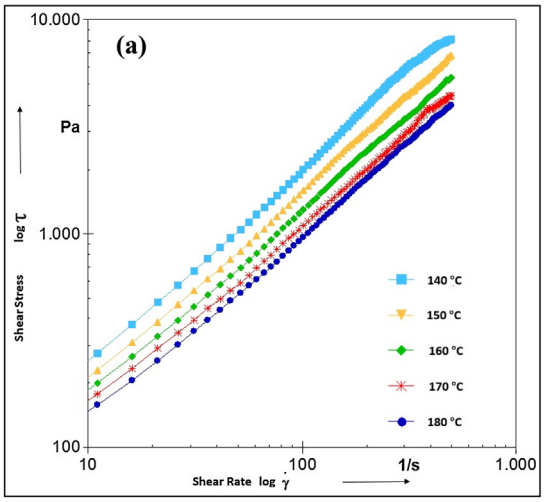

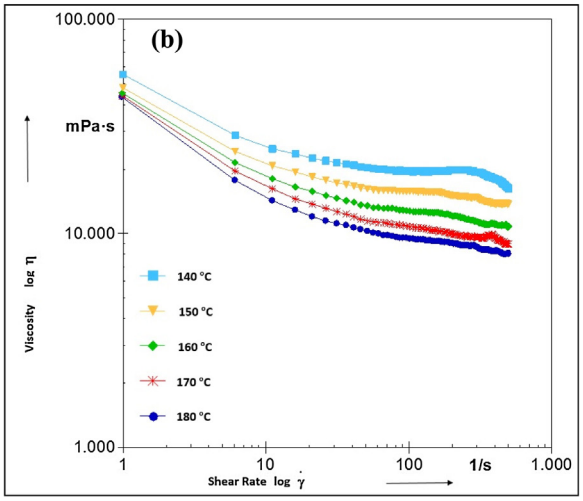

Fig. 3 – Temperature-dependent viscosity versus shear rate of Ti10Nb10Zr feedstock.

2.3. *Electrochemical tests*

For electrochemical evaluation, the cylindrical samples were polished to mirror finish in alcohol. The potentiodynamic scans were conducted using a flat cell, supplied by Gamry Instruments at room temperature. A standard three-electrode (reference, counter and working) technique was used for the measurement. The reference electrode used for the present experiment was saturated calomel electrode and the sintered alloy was chosen as the working electrode. The exposed area of the sintered sample to the solution was 8.01 mm^2. The electrochemical experiments were performed using a PC controlled Gamry Echem Analyst system software. Prior to the polariza-

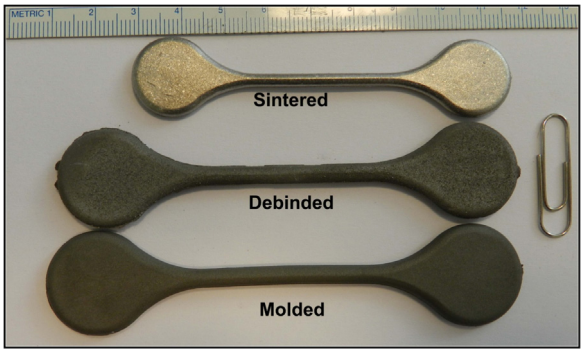

Fig. 4 – Photographs of molded, debinded and sintered Ti10Nb10Zr samples.

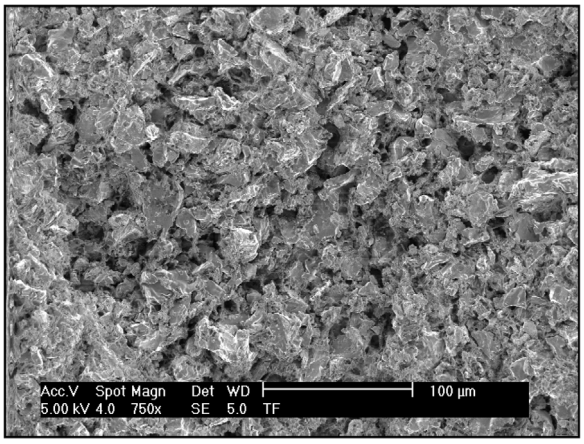

Fig. 5 – Fractured surface morphology of the Ti10Nb10Zr green sample (For interpretation of the references to colour in this figure legend, the reader is referred to the web version of this article).

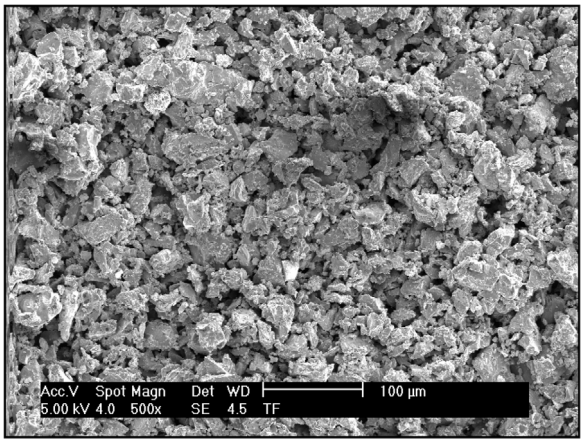

Fig. 6 – Fractured surface morphology of the Ti10Nb10Zr debinded (brown) sample.

Please cite this article in press as: Yemisci I, et al. Experimentation and analysis of powder injection molded Ti10Nb10Zr alloy: a promising candidate for electrochemical and biomedical application. J Mater Res Technol. 2019. https://doi.org/10.1016/j.jmrt.2019.08.046

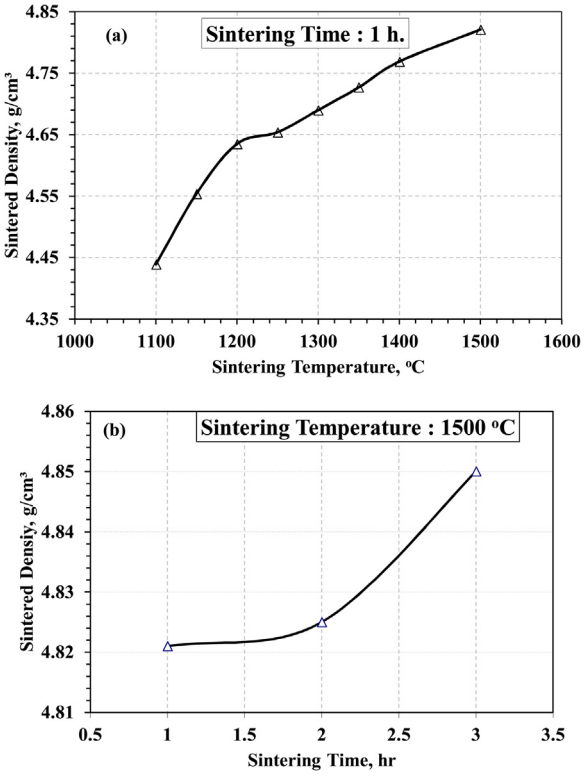

Fig. 7 – Effect of sintering temperature (a) and time (b) on sintered density of injection molded Ti10Nb10Zr samples.

tion test, each sample was stabilized for about the solution to get a stable open circuit potential (OCP). The potentiodynamic polarization tests were conducted minimum of three times at a constant scan rate of 1 mVs^{-1} in freely aerated % 3.5 NaCl. The potentiodynamic scans performed on the samples were plotted for voltage as a function of current density. The Tafel

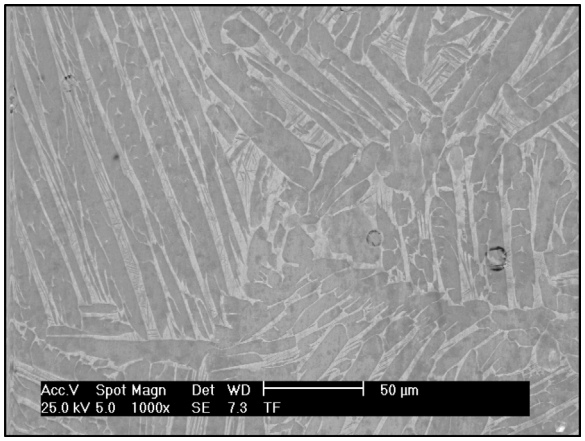

Fig. 9 – SEM micrograph of Ti10Nb10Zr sample sintered at 1500 °C for 3 h.

slopes were established from the active region of the corresponding anodic and cathodic curves. The critical parameters like corrosion potential (Ecorr), corrosion current (Icorr) and corrosion rate were evaluated from the polarization curves.

2.4. *In vitro and cell culture tests*

The samples (sintered 1500 °C, 1 h) as prepared were polished with sand papers of different grit sizes and rinsed ultrasonically in acetone, absolute alcohol and deionized water in turn for five times to remove any contamination and particulates. These samples were further used for in-vitro investigation in SBF and the process for preparation of SBF was as follows. The solution was prepared by dissolving reagent grade sodium chloride (NaCl), potassium chloride (KCl), calcium chloride dihydrate ($CaCl_2 \cdot 2H_2O$), magnesium chloride hexahydrate ($MgCl_2$ $6H_2O$), sodium hydrogen carbonate ($NaHCO_3$),

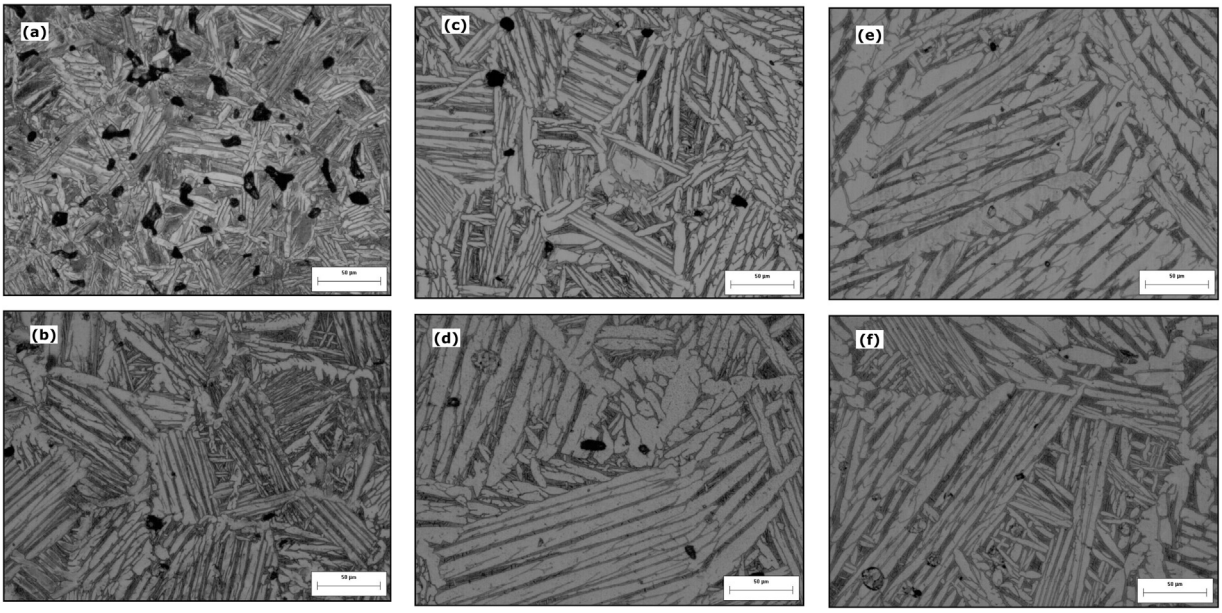

Fig. 8 – Optical micrographs of injection molded Ti10Nb10Zr samples, a) 1200 °C – 1 h, b) 1300 °C – 1 h, c) 1400 °C – 1 h, d) 1500 °C – 1 h, e) 1500 °C – 2 h and f) 1500 °C – 3 h.

Please cite this article in press as: Yemisci I, et al. Experimentation and analysis of powder injection molded Ti10Nb10Zr alloy: a promising candidate for electrochemical and biomedical application. J Mater Res Technol. 2019. https://doi.org/10.1016/j.jmrt.2019.08.046

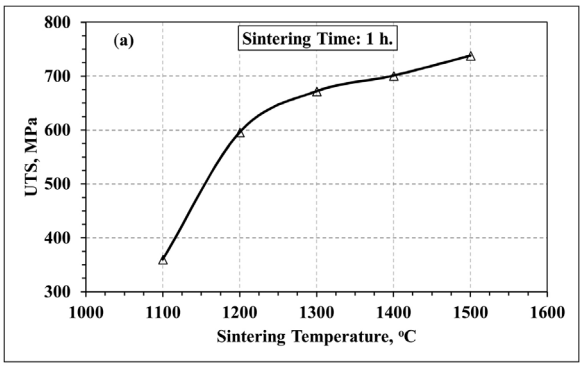

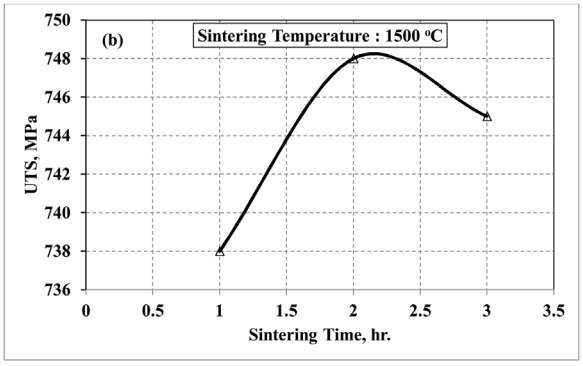

Fig. 10 – Effect of sintering temperature (a) and time (b) on ultimate tensile strength of injection molded Ti10Nb10Zr samples.

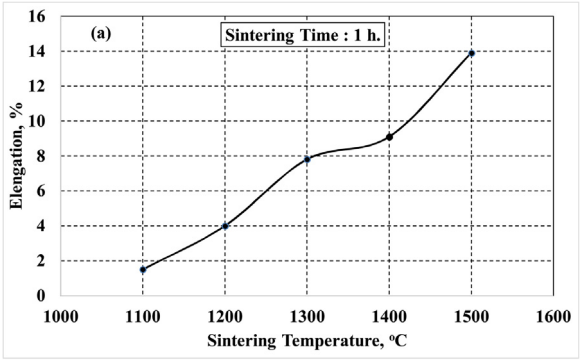

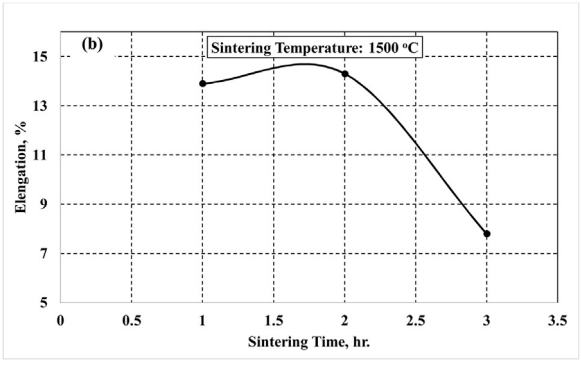

Fig. 11 – Effect of sintering temperature (a) and time (b) on elongation of injection molded Ti10Nb10Zr samples.

dipotassium hydrogen phosphate trihydrate (K_2HPO_4 $3H_2O$), sodium sulphate (Na_2SO_4) in deionized water. Then the solution was buffered to physiological pH 7.4 at 37.5 °C by both hydrochloric acid (HCl) and tris (hydroxymethyl)-aminomethane ($(CH_2OH)3CNH_2$). The ion concentration of the SBF is shown in Table 2. The sintered samples were immersed in sealed test tubes containing 20 ml of SBF for 7 and 15 days. The experiment was performed in a laboratory water bath that was maintained at a constant temperature of 37.5 °C and subjected to a continuous vibrating motion to help maintain uniform ion concentration. After immersion in SBF for various periods, the sintered samples were retrieved, gently rinsed with distilled water, and dried at 45 °C for 1 day. The surface of the samples was finally examined by SEM.

Biocompatibility assessments were carried by direct interaction of the material with 3T3 mouse embryonic fibroblasts. 3T3 fibroblast cells were maintained in DMEM (Dulbecco's Modified Eagle Medium-phenol red) (Gibco, Life Technologies, USA) supplemented with penicillin (100 U/mL)/streptomycin (100 μg/mL) (Gibco, Life Technologies, USA) solution and 10% of fetal bovine serum (Gibco, Life Technologies, USA) in T25 flasks. Cells were seeded at the density of 5000 cell/cm^2 and allow growing in incubator at 95% humidity and 5% CO_2 at 37 °C until to 80–90% of confluence. Cells were collected by trypsinization (Trypsin-EDTA 0.25%) (Gibco, Life Technologies, USA) and applied on to the materials in 6-well cell culture plates for 96 h with seeding density of 5×10^4 and maintained same environmental conditions. Cells were photographed by under a phase contrast inverted microscope (Olympus CK40)

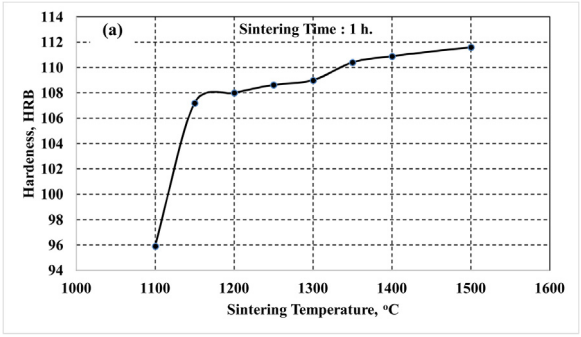

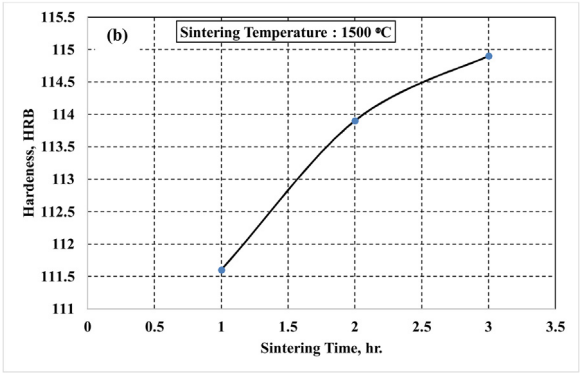

Fig. 12 – Effect of sintering temperature (a) and time (b) on hardness of injection molded Ti10Nb10Zr samples.

Please cite this article in press as: Yemisci I, et al. Experimentation and analysis of powder injection molded Ti10Nb10Zr alloy: a promising candidate for electrochemical and biomedical application. J Mater Res Technol. 2019. https://doi.org/10.1016/j.jmrt.2019.08.046

Table 3 – Mechanical properties of injection molded Ti10Nb10Zr alloys.

PIM - Ti10Nb10Zr alloy

Sintering conditions	Sintered density g/cm^3	Relative density %	UTS MPa	Elongation %	HardnessHRB
1100 – 1 h	4.43	90.7	360	1.5	95.9
1200 – 1 h	4.63	94.8	596	4	108
1300 – 1 h	4.69	96.1	672	7.8	109
1400 – 1 h	4.76	97.5	701	9.1	110.9
1500 – 1 h	4.82	98.7	738	13.9	111.6
1500 – 2 h	4.82	98.7	748	14.3	113.9
1500 – 3 h	4.85	99.3	745	7.8	114.8

using an image analysis system (Kameram, Micro System Ltd. Turkey) and harvested at 96 h. After 96-h of treatment, cell viability was assessed by trypan blue dye exclusion method. For this, 100 μl of %0.4 trypan blue solution (Gibco, Life Technologies, USA) was mixed with the equal amounts of cell suspension. And percentage of cell viability was analyzed and determined by automated cell counter (Bio-Rad TC20, USA).

Cell morphology was investigated by SEM after 96 h. Medium was removed; samples were washed with 0.15 M PBS buffer and fixed with 2.5% gluteraldehyte (4 °C). Samples were treated with 1% osmium tetroxide as secondary fixation, dehydrated with aceton series and incubated in amyl acetate. After critical point drying the cells on tested materials were imaged by the SEM.

3. Results and discussion

3.1. *Rheological properties of feedstock*

The evaluation of the feedstock rheological properties is based on viscosity and its shear sensitivity and temperature sensitivity. Fig. 3 illustrates the shear stress and viscosities of the feedstock at different shear rates and different temperatures of 130–180 °C. The feedstock viscosities as a function of temperature and shear-rate indicate the flowability of the feedstock within the mold cavity. As viscosity decreases, it becomes easier for the feedstock to flow in the mold cavity during PIM experiments. Fig. 3 shows that viscosity of feedstock decreases with increase in shear rate and increase in temperature. The results indicate that the feedstock has a typical shear thinning rheological behavior. In PIM, it is desirable that the viscosity of the feedstock should decrease quickly within increasing shear rate during molding and Fig. 3 allows in identifying the exact shear rate-temperature combinations required to get desired feedstock viscosity for injection molding. This shear rate — temperature sensitivity is especially important in producing complex parts [1,4].

Fig. 4 shows photographs of the molded, debinded and sintered samples. There are no defects evident such as blistering or slumping during molding, debinding, or sintering stages. Fig. 5 shows a typical fracture surface of a green sample shows that a good homogeneity was achieved for Ti10Nb10Zr samples. Scanning electron micrographs (SEM) taken at the center of the fractured green molded part show a uniform distribution of the binder throughout the part. A thin layer of the binder around almost all the particles can be seen which is considered useful for facilitating flow during the molding stage. Additionally, irregular shape of powders can be seen in these fractures of green parts. Fig. 6 shows a fracture surface of a brown sample (debinded) shows that the open pore channels were formed by the removal of polymeric binders. The formation of open pore channels allows the rapid removal of the remaining binder without cracking, blistering or swelling during thermal pyrolysis.

3.2. *Density and microstructural evolution*

The effect of sintering temperature and times on the sintered density of Ti10Nb10Zr sample is shown in Fig. 7. Fig. 7a shows that sintered densities of samples increase with increasing sintering temperatures from 1100 to 1500 °C. Density of 4.43 g/cm^3 was obtained for sampels sintered at 1100 °C for 1 h and a maximum sintered density of 4.82 g/cm^3 was obtained at sintering temperature of 1500 °C for 1 h. Furthermore, Fig. 7a indicates that densification becomes faster between 1100 and 1200 °C, in the β phase range with accompanying increase in diffusivity, reaching a maximum value. The microstructural analysis shows that a Widmanstatten like microstructure grows with the dissolution of the niobium particles from increasing of the sintering temperature. The boundaries between the angular Ti and Nb particles become diffuse. The dissolution of zirconium particles in both α and β areas is fast with the temperature increase. In the temperature range of 1100–1500 °C, the most noticeable microstructural features are the spreading of the α + β structure and the chemical homogenization of the alloy. The samples of the T10Nb10Zr alloy sintered at high temperatures of 1500 °C display a fine plate-like α + β structure with alpha on grain boundary.

Fig. 7b shows that sintered densities of samples increase with increasing sintering time. From Fig. 7b, it can be seen that at sintering temperature of 1500 °C for 3 h, maximum sintered density of 4.88 g/cm^3. Samples attained a maximum sintered density of at sintering temperature of 1500 °C for 3 h. This result shows that the sintering temperature and time improve the sintered density of samples.

Fig. 8 shows the optical micrographs of Ti10Nb10Zr samples sintered at 1200–1500 °C for 1 different sintering times. The porosity decreases and sintered density increases with increasing sintering temperature and time [2]. The matrix is α the small second phase particles are β in all samples. The sample was found to have a coarse acicular microstructure,

Please cite this article in press as: Yemisci I, et al. Experimentation and analysis of powder injection molded Ti10Nb10Zr alloy: a promising candidate for electrochemical and biomedical application. J Mater Res Technol. 2019. https://doi.org/10.1016/j.jmrt.2019.08.046

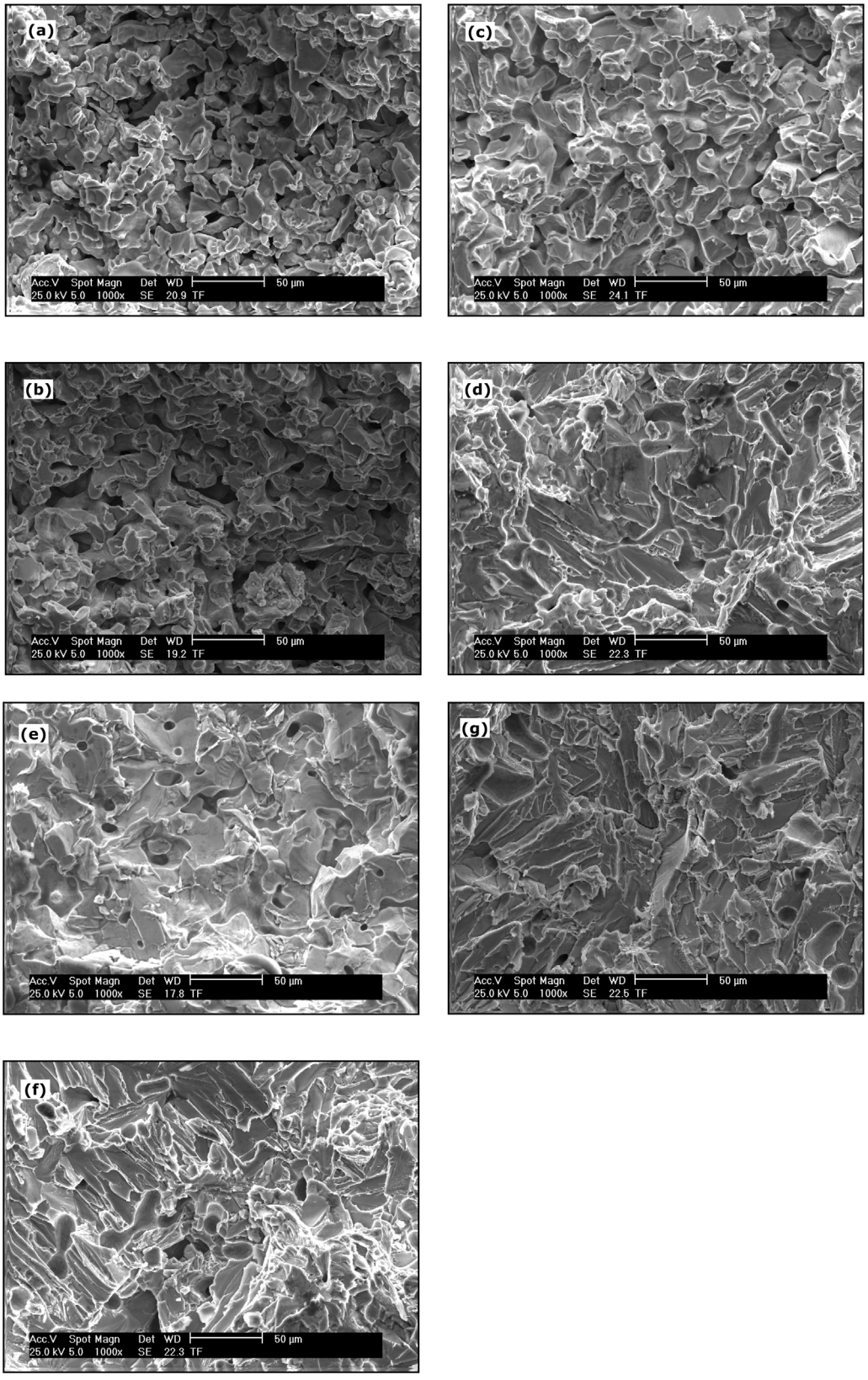

Fig. 13 – Fracture surface morphologies of injection molded Ti10Nb10Zr; a) 1100 °C – 1 h, b) 1200 °C – 1 h, c) 1300 °C – 1 h, d) 1400 °C – 1 h, e) 1500 °C – 1 h, f) 1500 °C – 2 h, and g) 1500 °C – 3 h.

Please cite this article in press as: Yemisci I, et al. Experimentation and analysis of powder injection molded Ti10Nb10Zr alloy: a promising candidate for electrochemical and biomedical application. J Mater Res Technol. 2019. https://doi.org/10.1016/j.jmrt.2019.08.046

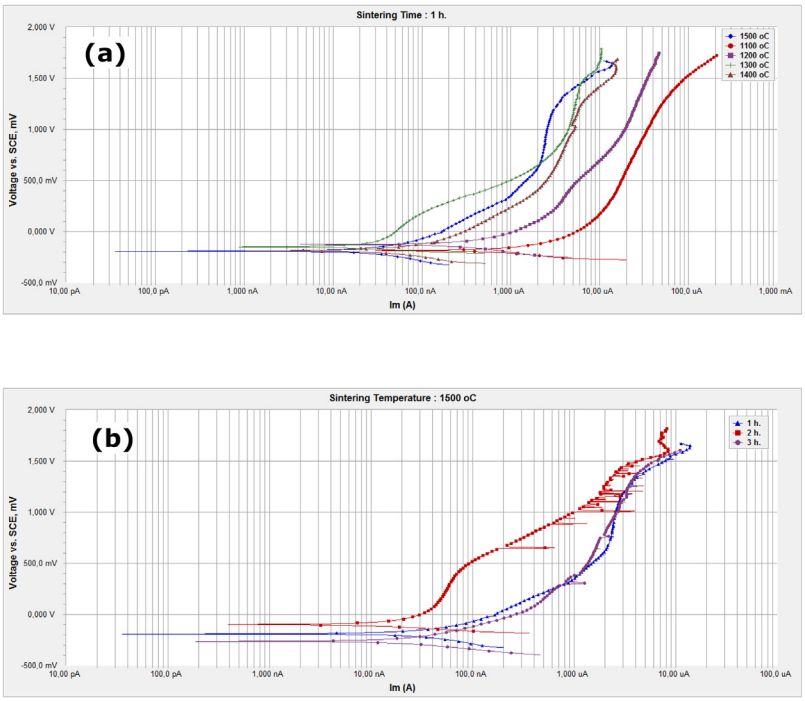

Fig. 14 – Effect of sintering temperature (a) and time (b) on Tafel curves for the sintered samples in 3.5% NaCl media.

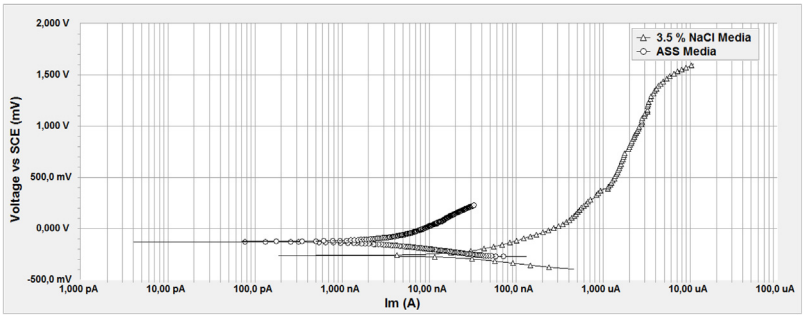

Fig. 15 – Tafel curves for the Ti10Nb10Zr samples in salty and ASS media.

Table 4 – Tafel extrapolation results of Ti10Nb10Zr sample in salty and ASS media.

	Beta A (mV/decade)	Beta C (mV/decade)	I_{corr} (nA)	E_{corr} (-mV)	Corr. rate (10^{-3} mpy)
3.5 %NaCl media	263	127	28.50	263.0	139.3
ASS media	368.9	145.1	4.13	129.0	20.19

Table 5 – Element concentrations of sintered Ti10Nb10Zr sample in SBF.

	Elements (wt.%)					
	Ti	Na	P	Cl	K	Ca
7 days	75.87	7.33	5.39	3.17	4.58	3.66
15 days	61.13	9.11	9.62	7.23	6.4	6.51

revealing α grains with intergranular β-phase. The percentage of α-phase in the alloys depend on the sintering conditions. A lower sintering temperature affects porosity and the amount of α-phase, which appears precipitated at the grain boundaries, darker than β-phase. Samples sintered for high temperatures and times possessed Widmanstatten microstructure, which consisted of α and β lamellae. The β grains were outlined by the α phase and the contained several colonies of α and β lamellae. The colonies had α and β lamellae aligned in the same orientation. The β grains, α colonies and α

Please cite this article in press as: Yemisci I, et al. Experimentation and analysis of powder injection molded Ti10Nb10Zr alloy: a promising candidate for electrochemical and biomedical application. J Mater Res Technol. 2019. https://doi.org/10.1016/j.jmrt.2019.08.046

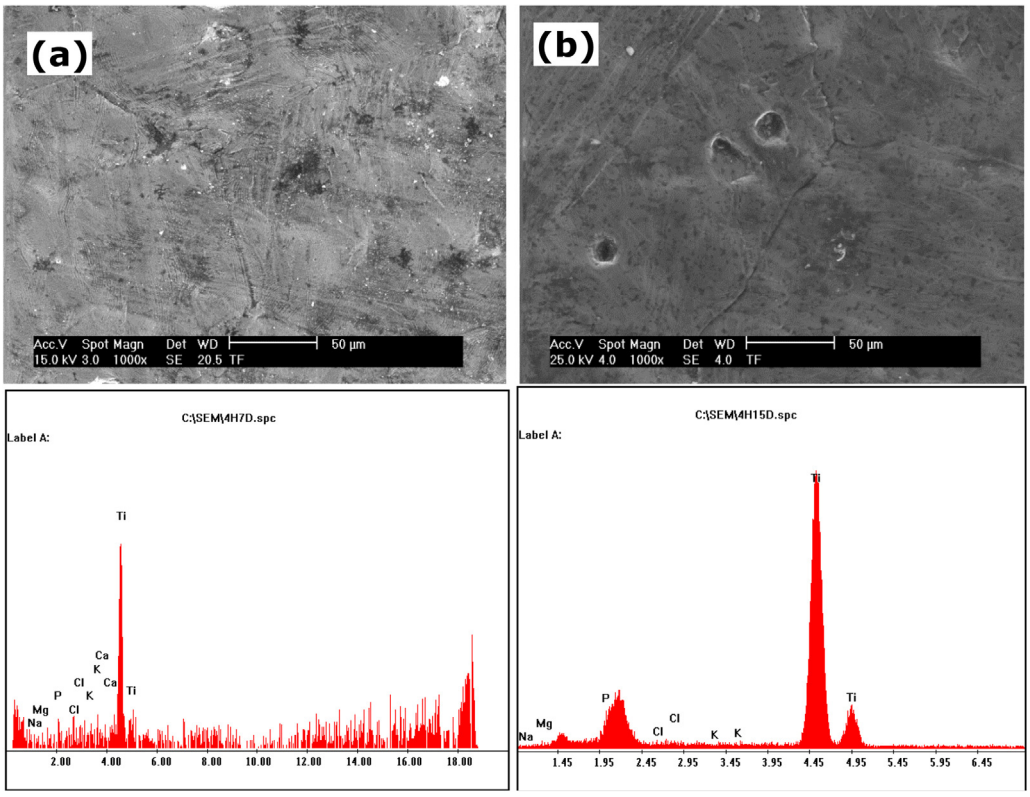

Fig. 16 – SEM morphologies and EDS spectra of the surfaces of Ti10Nb10Zr samples: (a) 7 and (b) 15 days immersion in SBF.

phase thickness in the β grains had much effect on properties (Fig. 9) [2–4,6].

3.3. *Mechanical properties*

The effect of sintering temperature and time on the ultimate tensile strength and elongation of Ti10Nb10Zr samples are shown in Figs. 10 and 11. The ultimate tensile strength and elongation were increased with sintering temperature and time. Thus, pores are closed and theoretical densities increased at high sintering temperatures and time [2–4]. For the samples were sintered at 1100 °C for 1 h; a maximum ultimate tensile strength and elongation 360 MPa and 1.5% was reached, respectively. Samples attained a maximum ultimate tensile strength and elongation of 738 MPa and 13.9% at sintering temperature of 1500 °C for 1 h, respectively. Samples attained an ultimate tensile strength and elongation of 745 MPa and 7.8% at sintering temperature of 1500 °C for 3 h. This result shows that the sintering temperature and time improve the ultimate tensile strength and elongation of samples. Additionally, with increase in sintering times, elongation was decreased.

The effect of sintering temperature and time on the hardness of injection molded Ti10Nb10Zr sample is shown in Fig. 12. The hardness was increased with sintering temperature and time [2]. The samples were sintered at 1100 °C for 1 h; a maximum hardness of 95.5 HRB was reached. Samples attained a maximum hardness of 111.6 HRB at sintering temperature of 1500 °C for 1 h. The hardness of samples sintered at 1500 °C was higher than those sintered at 1100 °C. From Fig. 12b it can be seen that at sintering temperature of 1500 °C for 3 h, maximum hardness of 114.8 HRB. Comparative mechanical properties of the samples processed under different sintering conditions are shown in Table 3.

Fig. 13 shows the fracture surfaces of the Ti10Nb10Zr samples. The samples sintered at lower temperatures still show particulate features (Fig. 13a–d). At lower temperatures, main fracture mode is the separation of particles and necking areas where bonding between particles took place during sintering. With increasing sintering temperature, increased ribbed features are seen on the fractured surfaces indicating some grains failed in ductile mode (Fig. 13 e–g). In samples sintered at 1500 °C with increase in sintering time from 1 h to 3 h, changes the fracture mode from dimpled to intergranular mode, thereby resulting in lowering of ductility (Fig. 13 e–g). [8,13,16].

3.4. *Electrochemical properties*

Fig. 14 shows the extrapolation of the Tafel curves the corrosion potential, Ecorr (measured relative to SCE), Tafel slopes in the anodic and cathodic region and corrosion current density (icorr) were determined. In general, irrespective of the sintering temperature and time, a significant improvement in the corrosion resistance for the sintered samples was observed. This can be attributed to the enhanced densification achieved by the 1500 °C sintered samples. Additionally, with increase in sintering temperature and sintering time the corrosion resis-

Please cite this article in press as: Yemisci I, et al. Experimentation and analysis of powder injection molded Ti10Nb10Zr alloy: a promising candidate for electrochemical and biomedical application. J Mater Res Technol. 2019. https://doi.org/10.1016/j.jmrt.2019.08.046

tance improved [26–29]. Fig. 15 shows the extrapolation of the Tafel curves, the corrosion potential, E_{corr} (measured relative to SCE), Tafel slopes in the anodic and cathodic region and corrosion current density (I_{corr}) were determined and given in Table 4. Plus explain how the corrosion rate increased Furthermore, the sintered samples showed relatively higher corrosion rate of 139.4 in 3.5% NaCl solution when compared to 20 in ASS media indicating that the samples were more resistive to corrosion in the ASS media (Table 4). According to Tafel curves, in ASS the corrosion rate of Ti10Nb10Zr samples is lower than in salty solution media. The environment constituted by the salty solution is more aggressive for samples than the ASS solution. Ti10Nb10Zr samples show low corrosion rate in ASS environment. The Ti10Nb10Zr alloy exhibited excellent corrosion resistance in 3.5%NaCl and ASS media. Compared with 316 l stainless steel and CoCrMo alloys, the pitting resistance was significantly improved, indicating that the alloy is less likely to cause failure and ion release by pitting [6].

3.5. *SBF immersion and cell culture properties*

SEM morphologies of the sample surfaces after immersion in the SBF for various times are shown in Fig. 16. It can be seen that after 7 days immersion, many globular apatite particles have grown on the surface of the samples. The content of Ti10Nb10Zr is scarcely observed on the surface and only Ca and P can be examined on the biomaterial surfaces after immersion for 7 days. It reveals that the apatite areas containing Ca and P on the biomaterials surfaces are formed. With the increase of immersion time, the quantity and size of the apatite particles increase gradually. After 15 days immersion, the surface of the samples is more covered with apatite [8,30]. The EDS spectrum in Fig. 16 and element concentrations in Table 5 show that the dominating elements on the surfaces of sample are Na, Mg, P, Cl, K and Ca after immersion in SBF for 7 and 15 days. In the initial immersion in SBF, all ions on the biomaterial surfaces are dissolved into SBF; however, the supersaturation of ions is low. The crystal nuclei adsorb the ions from their own surrounding environment and develop in their growth process [10,31].

Fig. 17 shows the morphologies of the cells on samples after 96 h of cell culture. Cells were flattened and well spread across the Ti10Nb10Zr sample surfaces after 96 h, as shown in Fig. 17 at different magnifications. On sample surfaces, cells were seen to adhere to surface (e.g. filopodia), and were connected to the substrate neighboring cells. On the sample surface cell growth was less pronounced with limited establishment of cell spreading being seen after 96 h of culture. Fig. 18 shows the Trypan blue results of cell represented at the end of 96 h exposition for Ti10Nb10Zr samples. When comparing the test results, control sample (inert glass slide) with Ti10Nb10Zr is the best biocompatible alloy, and all groups were very close to Ti10Nb10Zr. Our cell culture data indicated that Ti10Nb10Zr samples are biocompatible.

Fig. 19 shows the phase contrast microscopic examination revealed not significant differences in the cell growth behavior for 96 h near the surfaces of Ti10Nb10Zr. Black areas at the corners of the photographs are the borders and shadows of the test samples. As shown in Fig. 19 for the Ti10Nb10Zr surface, the fibroblasts near the sample with the shape of shuttle and/or elongated polygon, which are the normal individual form of the 3T3 mouse fibroblast cells [32,33].

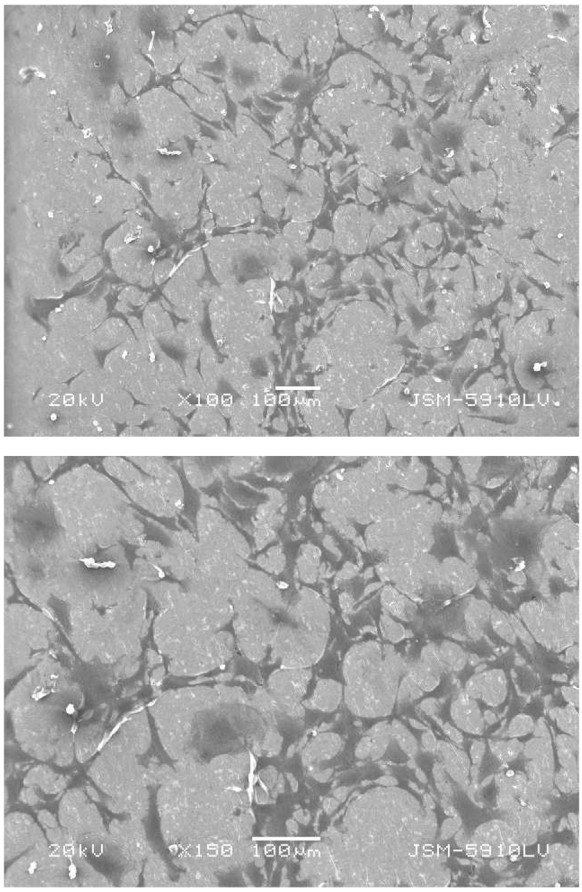

Fig. 17 – SEM micrographs of cell morphology after 96 h of culture on sample surfaces at two magnifications.

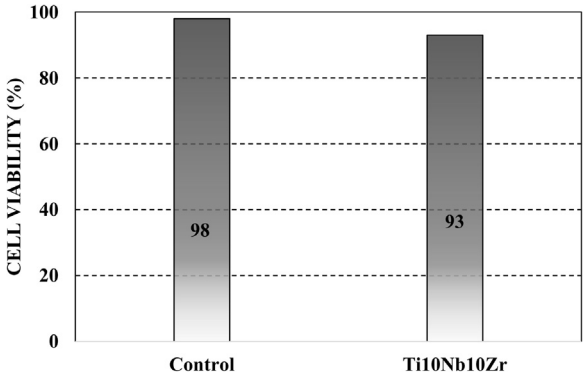

Fig. 18 – Cell viability on surface of control and Ti10Nb10Zr samples in 96 h.

Please cite this article in press as: Yemisci I, et al. Experimentation and analysis of powder injection molded Ti10Nb10Zr alloy: a promising candidate for electrochemical and biomedical application. J Mater Res Technol. 2019. https://doi.org/10.1016/j.jmrt.2019.08.046

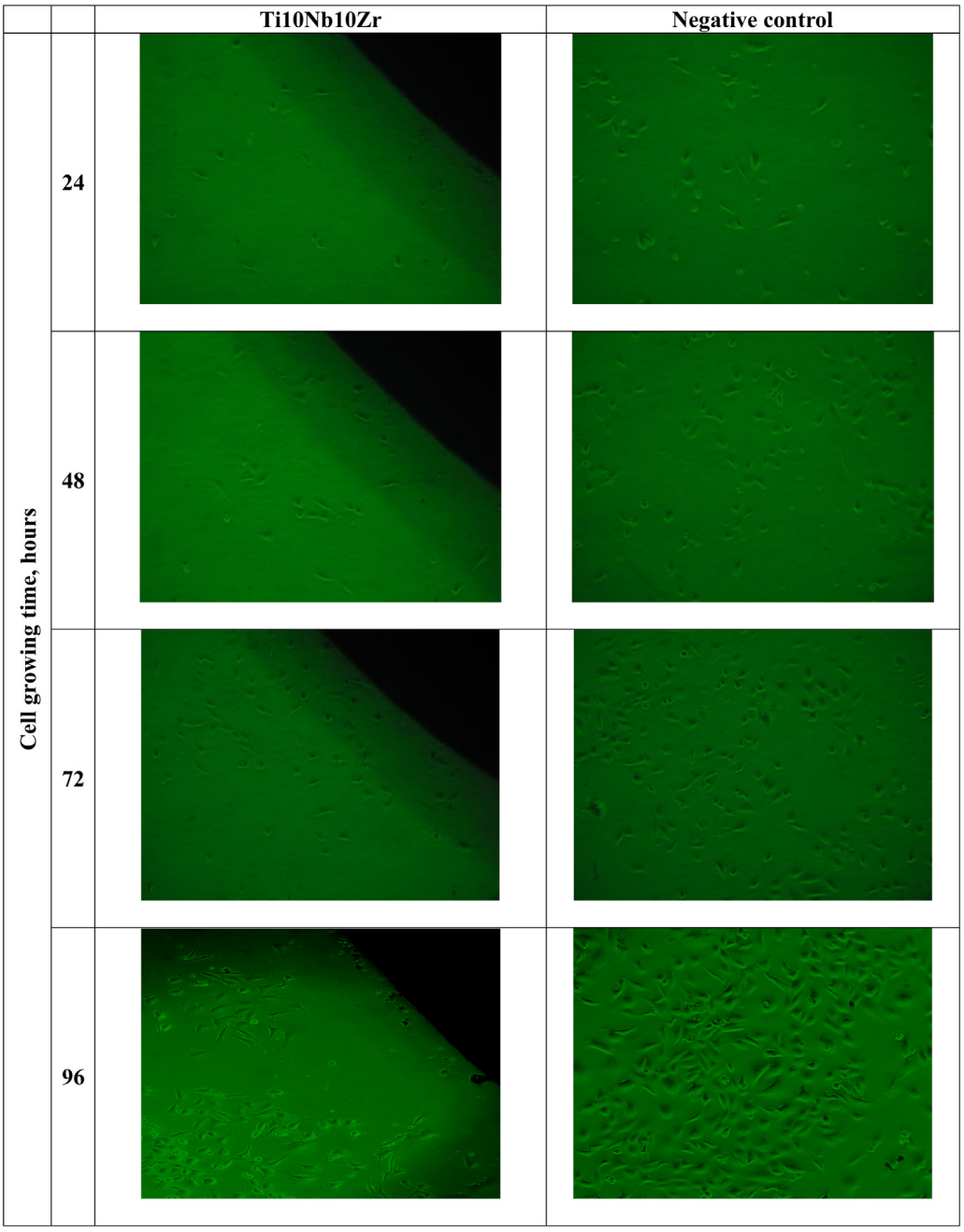

Fig. 19 – Phase-contrast micrographs of fibroblasts cultured on Ti10Nb10Zr and negative control for different times (24–96 h).

4. Conclusions

As conculussion, Ti-Zr-Nb alloys have shown many significant advantages as potential implant materials. Experimental results show that the sintering temperature and sintering time increased sintered density, ultimate tensile strength, elongation and hardness of PIM-Ti10Nb10Zr samples. Microstructural evolution and mechanical properties of PIM-Ti10Nb10Zr samples could be controlled easily in vacuum atmosphere. The sintered density, ultimate tensile strength, elongation, and hardness were 99%, 748 MPa, 14% and 115 HRB, respectively. Electrochemical test indicated that the samples showed higher corrosion rate in 3.5% NaCl solution than in ASS media. Furthermore, the SBF immersion tests indicate that the Ca-deficient apatite is bone-like apatite with excellent bioactivity. The results of cell culture show that injection molded Ti10Nb10Zr samples are well tolerated by the 3T3 mouse fibroblasts, which showed normal morphology and attached onto the samples over the incubation times. The results discussed in this work indicate that the PIM-Ti10Nb10Zr alloys can be promising candidates for application as biomedical materials due to their high strengths, good corrosion resistance and high bioactivity.

Please cite this article in press as: Yemisci I, et al. Experimentation and analysis of powder injection molded Ti10Nb10Zr alloy: a promising candidate for electrochemical and biomedical application. J Mater Res Technol. 2019. https://doi.org/10.1016/j.jmrt.2019.08.046

Conflicts of interest

The authors declare no conflicts of interest.

Acknowledgements

This work has been supported by Scientific Research Project Program of Marmara University (BAPKO) (Project No. FEN-B-100616-0274).

REFERENCES

[1] German RM, Bose A. Injection molding of metals and ceramics. Metal Powder Industries Federation; 1997.
[2] Ergul E, Gulsoy HO, Gunay V. Powder Metall 2009;52:65–71.
[3] Guo SB, Qu XH, He XB, Zhou T, Duan BH. J Mater Process Technol 2006;173:310–5.
[4] Wu Y, Wang R, Kwon Y, Park S, German RM. Int J Pow Metall 2006;42:59–65.
[5] Nyberg E, Miller M, Simmons K, Weil KS. Mater Sci Eng C 2005;25:336–42.
[6] Yan XH, Ma J, Zhang Y. Sci China-Phys Mech Astron 2019;62. Article Number: 996111.
[7] Henriques VAR, Galvani ET, Petroni SLG, Paula MSM, Lemos TG. J Mater Sci 2010;45:5844–50.
[8] Gulsoy HO, Gulsoy N, Calısıcı R. Biomed Mater Eng 2014;24:1861–73.
[9] Dehghan-Manshadi A, Bermingham MJ, Dargusch MS, StJohn DH, Qian M. Powder Technol 2017;319:289–301.
[10] Li Y, Yang C, Zhao H, Qu S, Li X, Li Y. Materials 2014;7:1709–800.
[11] Brailovski V, Prokoshkin S, Gauthier M, Inaekyan K, Dubinskiy S. J Alloys Compd 2013;577:413–71.
[12] Meng Q, Guo S, Liu Q, Hu L, Zhao X. Prog Nat Sci 2015;25:229–35.
[13] Zhao D, Chang K, Ebel T, Qian M, Willumeit R, Yan M, et al. J Mech Behav Biomed Mater 2013;28:171–82.
[14] Gerling R, Schimansky F. Mater Sci Eng A 2002;329:45–9.
[15] Thian ES, Loh NH, Khor KA, Tor SB. J Biomed Mater Res 2002;63:79–85.
[16] Itoh Y, Uematsu T, Sato K, Miura H, Niinomi M. J Jpn Soc Pow Metal 2008;55:720–5.
[17] Kafkas F, Ebel T. J Alloys Compd 2014;617:359–66.
[18] Hamidi MFFA, Harun WSW, Samykano M, Ghani SAC, Ghazalli Z, Ahmad F, et al. Mater Sci Eng C 2017;78:1263–76.
[19] Yılmaz E, Gökçe A, Findik F, Hamit Özkan G, Gulsoy HÖ. J Therm Anal Calorim 2018;134:7–14.
[20] Zhao D, Chang K, Ebel T, Qian M, Willumeit R, Yan M, et al. J Mech Behav Biomed Mater 2013;28:171–82.
[21] Zhao D, Chang K, Ebel T, Nie H, Willumeit R, Pyczak F. J Alloys Compd 2015;640:393–400.
[22] Nagaram AB, Ebel T. Key Eng Mater 2016;704:334–42.
[23] Bidaux J-E, Closuit C, Rodriguez-Arbaizar M, Zufferey D, Carreño-Morelli E. Powder Metall 2013;56:263–6.
[24] Hussein AH, Gepreel MA, Gouda MK, Hefnawy AM, Kandil SH. Mater Sci Eng C 2016;61:574–8.
[25] Sidambe AT. Materials 2014;7:8168–88.
[26] Xin F, Jian C, Peng ZJ. Trans Nonferrous Met Soc China 2009;19:347–52.
[27] Balla VK, Bodhak S, Bose S, Bandyopadhyay A. Acta Biomater 2010;6:3349–59.
[28] Tang YC, Katsuma S, Fujimoto S, Hiromoto S. Acta Biomater 2006;2:709–11.
[29] Han MK, Kim JY, Hwang MJ, Song HJ, Park YJ. Materials 2015;8:5986–6003.
[30] Bai Y, Deng Y, Zheng Y, Li Y, Zhang R, Lv Y, et al. Mater Sci Eng C 2016;59:565–76.
[31] Tsutsumi Y, Bartakova S, Prachar P, Suyalatu, Migita S, Doi H, et al. J Electrochem Soc 2012;159:C435–40.
[32] Xiong J, Li Y, Wang X, Hodgson P, Wen C. Acta Biomater 2008;4:1963–8.
[33] Catauro M, Bollino F, Papale F. J Biomed Mater Res Part B Appl Biomater 2014;102:4473–9.

Please cite this article in press as: Yemisci I, et al. Experimentation and analysis of powder injection molded Ti10Nb10Zr alloy: a promising candidate for electrochemical and biomedical application. J Mater Res Technol. 2019. https://doi.org/10.1016/j.jmrt.2019.08.046